Association of *E. coli* Nissle with insect-parasitic nematode *Steinernema hermaphroditum*

Victoria Chen[1,2*], John P. Marken[2*], Richard M. Murray[2], Mengyi Cao[2,3#]

[1] Department of Biological Engineering, Massachusetts Institute of Technology, Cambridge, Massachusetts 02139

[2] Division of Biology and Biological Engineering, California Institute of Technology, Pasadena, CA 91125

[3] Division of Biosphere Sciences and Engineering, Carnegie Institution for Science, Pasadena, CA 91125

[*]Denotes equal contributions

[#] To whom correspondence may be addressed:

Mengyi Cao: mcao@carnegiescience.edu, mengyi.cao77@gmail.com

Running title: *Steinernema* nematode and *E. coli* Nissle interaction

Keywords: *E. coli* Nissle, entomopathogenic, nematode, *Steinernema hermaphroditum*, bacterial colonization

Abstract

Steinernema species are soil-dwelling and insect-parasitic nematodes that associate with symbiotic *Xenorhabdus* bacteria. During the infective juvenile (IJ) stage, *Steinernema* nematodes package species-specific *Xenorhabdus* bacteria in the anterior intestinal pockets. The nematodes can survive in the soil for months as they seek insect prey. The mechanisms of how these nematodes associate with environmental microbes other than their *Xenorhabdus* symbionts is barely known. Here, we report a new mechanism of *E. coli* Nissle (EcN) association with the nematode *Steinernema hermaphroditum.* We show that EcN cells are enclosed and lysed in at least four pairs of coelomocytes, suggesting these immune cells respond to bacterial invasion. During the IJ stage of nematode development, EcN cells localize to posterior intestinal vacuoles and enter the inter-cuticular space, where they proliferate, aggregate, then lyse. EcN cells expressed proteins in the cell lysates were maintained in the nematode cuticle over eight weeks in non-sterile soil. These observations suggest sequential steps of EcN colonization in the host nematodes involving an immune response that is distinctive from interactions with mutualistic symbiont. Our work establishes a novel framework of nematode-bacteria interaction with potential applications in environmental bioengineering.

Introduction

Animal tissues create complex, compartmentalized spaces that provide abiotic and biotic environments capable of selecting and maintaining mutualistic microorganisms while antagonizing pathogenic ones. Reciprocally, microbes develop within these host-derived environments, shaping the identity of the niches they occupy. This process of microbial modulation of the local environment, known as niche construction, can drive long-term coevolution. In contrast, pathogens can exploit unoccupied niches, leading to opportunistic infections and niche deconstruction (Baquero *et al.*, 2021). Identifying and characterizing novel niches within animal hosts, as well as the dynamic interactions of microbes within these microenvironments, are crucial for understanding the mechanisms and consequences of host-microbe crosstalk. Binary symbioses, involving a single core symbiont and a single animal species, provide efficient models for revealing the temporal and spatial dynamics of symbiont colonization within specific host cells and tissues. The niche-specific interactions observed in diverse binary symbiosis models are critical for host development and ecosystem health (Nyholm and McFall-Ngai, 1998; Stilwell *et al.*, 2018; Maire *et al.*, 2020; Tivey *et al.*, 2022). While binary symbiosis often involves colonization by a single microbial species within a specialized organ, additional genera or species can sometimes associate with distinct tissues, maintaining spatial separation from primary symbionts (Dale and Moran, 2006; Nyholm and McFall-Ngai, 2021). The relatively simple composition of these natural microbiomes makes such animal models advantageous for studying multiple types of host-microbe interactions simultaneously.

The entomopathogenic (EPN, insect-parasitic) nematode *Steinernema spp* maintains a stable association with mutualistic *Xenorhabdus* bacteria in a binary symbiosis. Each generation of nematodes acquires their symbiotic bacteria from the external environment (semi-horizontal) while a maternal factor can influence the bacterial colonization of the next generation (semi-vertical). The intestine of *Steinernema* nematodes contains compartmentalized niches where multiple microenvironments enable the attachment, persistence, and proliferation of *Xenorhabdus* bacteria (Chaston *et al.*, 2013) (Fig. 1A and Fig. 1B). *Xenorhabdus* bacteria first attach to the anterior intestinal ceacum (AIC) in juveniles, while nematodes feed on bacteria, molt through four juvenile stages (J1-J4) and become adults to reproduce. Signals from overcrowding and lack of food source induce the J2 stage of juveniles to molt into IJs through an alternative developmental pathway. During IJ development, the symbiotic bacteria first localize to the pharyngeal intestinal valves (PIV) in the pre-IJs. These narrow pouches restrict bacterial colonization to a few cells per animal. During the infective juvenile (IJ) stage, symbiotic bacteria migrate into the anterior intestinal pocket, termed the receptacle (Fig. 1B). The multiple intestinal tissues involved in the colonization events, including AIC, PIV, and the receptacle, are proposed to provide specific nutrients, signaling molecules, and physical restrictions to select the specific species or strain of *Xenorhabdus* bacteria.

Steinernema are soil-dwelling nematodes that also encounter other species of microbes from their natural environment. Bacteria from multiple genera, termed the ‘pathobiome’, are found to frequently associate with certain *Steinernema* spp and potentially contribute to entomopathogenic (insect-killing) activities (Ogier *et al.*, 2020).

Despite its generalization of pathobiomes among multiple *Steinernema* species, the frequency, localization, and molecular mechanisms of pathobiome association is unknown. Little else is known about other environmental microbes -- either pathogenic, mutualistic, or commensal -- that interact with EPNs. This knowledge gap limits the full application of *Steinernema* as a symbiosis model and its applications in bioengineering. Therefore, understanding the spatial and temporal interactions of pathogens and commensals in *Steinernema* provides a foundational framework for novel modes of symbiotic interactions.

Engineered biocircuits, such as bacterial biosensors, provide valuable tools for monitoring the spatial and temporal dynamics of specific environmental patterns. *Escherichia coli* is the most established bacterial species for engineering and is a leading candidate for biosensing applications across diverse niches, including complex microenvironments in cell-cell signaling in animals and soil matrices with sophisticated heterogeneity (Valle *et al.*, 2021). *E. coli* is commonly associated with the animal intestinal tract (host-dependent) and circulates through the soil and water environment (host-independent) via a biphasic lifestyle (Fig. 1C). Certain *E. coli* strains can persist in soil environments, where they influence indigenous microflora encountered by insects and soil-dwelling nematodes (Elsas *et al.*, 2010). Given the diversity of *E. coli* strains—from human pathogens to beneficial probiotics—understanding strain-specific behaviors within a given niche is critical for selecting appropriate candidates for engineering sustainable biosensors. The *E. coli* Nissle 1917 (EcN) strain, originally isolated from a soldier who survived a *Shigella* epidemic, is known to interact with the mammalian

111 intestinal epithelium and mucosal immune system, antagonize pathogenic
112 enterobacteria, and confer probiotic benefits in human(Sonnenborn, 2016).
113 In this study, we investigated the interactions of multiple *E. coli* strains with the
114 entomopathogenic nematode *Steinernema hermaphroditum*. We discovered that EcN
115 localizes within previously undocumented cell and tissue types in *S. hermaphroditum*,
116 including immune cells (coelomocytes), posterior intestinal tissues, and inter-cuticular
117 spaces. These snapshots of EcN localization in nematodes suggest a sequential
118 process of cell- and tissue-specific microbe-host interactions synchronized with infective
119 juvenile (IJ) development. Notably, EcN colonization occurs in spatially distinct tissues
120 from those occupied by *Xenorhabdus*, the nematode's native symbiont. Our findings
121 establish *E. coli* Nissle–*S. hermaphroditum* interactions as a new platform for
122 engineering *E. coli*-encoded biosensors to monitor niche-specific symbiotic interactions.
123 *S. hermaphroditum* offers a promising delivery system for such biosensors due to its
124 transparency, short life cycle in vitro, and bacterivorous nature (Bracho *et al.*, 2016;
125 Hwang *et al.*, 2017; Rutter *et al.*, 2019). Furthermore, we observed that proteins from
126 EcN lysates persist on the nematode cuticle, highlighting the potential for protein-based
127 biosensors to be carried by *S. hermaphroditum* for monitoring soil ecosystem.
128
129 **Experimental Procedures**
130 **Construction of fluorescent *E. coli* Nissle strains with mScarlet-I.** Genetic
131 constructs for constitutive expression of either green fluorescent protein (sfGFP) or red
132 fluorescent protein (mScarlet-I) were assembled using the 3G assembly method
133 (Halleran *et al.*, 2018) with standard parts from the MoClo modular cloning toolkit

134 (Iverson *et al.*, 2016). The resulting constructs were cloned into the “KL” genome
135 integration vector from the pOSIP one-step genome integration system (St-Pierre *et al.*,
136 2013) , which facilitates integration at the phage 186 integrase attachment site in the *E.*
137 *coli* genome. Plasmids were transformed into chemically competent *E. coli* strains
138 (Nissle 1917, CSH50, and BW25113) using a standard heat shock protocol. Briefly, 50
139 µL of competent cells were mixed with 100 ng of plasmid DNA, incubated on ice for 30
140 minutes, heat shocked at 42 °C for 45 seconds, and then placed back on ice for 2
141 minutes. Cells were allowed to recover in 950 µL of SOC medium at 37 °C with shaking
142 for 1 hour before being plated on LB agar plates containing kanamycin (50 µg/mL) to
143 select for successful integrants. Plates were incubated at 37 °C overnight. Resulting
144 transformants were screened via colony PCR on the integration locus using the
145 standard screening primers from (St-Pierre *et al.*, 2013) and Sanger sequenced to
146 validate the successful integration.
147
148 **Liver-kidney agar plates.** The recipe for Liver-kidney agar was adapted from (Flores-
149 Lara *et al.*, 2007): 50 g of pork liver and 50 g of pork kidney were blended in 250 mL
150 distilled water until smooth. 2.5 g of NaCl, 7.5 g agar, 250 mL of water, and the liver-
151 kidney solution was transferred to a flask, then autoclaved and cooled in a 55°C water
152 bath. To avoid contamination, the liver-kidney agar was supplemented with kanamycin
153 (50 µg/mL) and poured into 60 x 15mm Petri plates under a fume hood. The agar was
154 continuously swirled before pouring to avoid pouring any larger chunks.
155

156 ***S. hermaphroditum* axenic egg extraction and colonization assay.** The method for
157 axenic egg extraction for *S. hermaphroditum* was adapted from (Murfin *et al.*, 2012).
158 Liquid cultures of symbiotic bacterium *X. griffiniae* (HGB2511) were grown overnight in
159 LB media that were kept in the dark and added to lipid agar plates (Vivas and Goodrich-
160 Blair, 2001). Plates were cultured for 48 hours to form a bacterial lawn. To prepare
161 axenic (germ-free) eggs, conventional IJs (exclusively propagated through insects) were
162 added to the lawns of *X. griffiniae* (HGB2511) and incubated for 2-3 days to grow to
163 gravid adults. Nematodes were washed off the bacterial lawn with water and then
164 transferred to 50 mL conical tubes (Falcon, Corning, NY) and centrifuged at 3000 rpm
165 for 2 minutes. The supernatant was removed using a vacuum, and 2 mL of a lysis
166 solution (2.4 mL 8% bleach, 500 µL 5M KOH, 7.1 mL water) was added to lyse the
167 gravid adult hermaphrodites. Nematodes were incubated in the lysis solution for 5
168 minutes at room temperature and mixed several times per minute by inverting. The
169 solution was then centrifuged at 3000 rpm for two minutes, and the lysis solution was
170 removed using a vacuum. Nematode eggs were washed thrice with 10 mL of LB
171 medium. Their density was assessed by viewing the number of IJs in 2 µL spots under a
172 stereoscope. Approximately 500 eggs were added to the prepared liver-kidney or lipid
173 agar plates, with or without bacterial lawn of *X. griffiniae* expressing GRP (Thomas *et*
174 *al.*, 2024) or *E. coli* expressing RFP, and incubated at 25℃ for 1 week. Plates were then
175 moved to 100 x 25mm Petri dishes filled with 10-15 mL of water to trap infective
176 juveniles. Colonization phenotypes and frequencies were assessed using fluorescence
177 microscopy (See Microscopy and Image Acquisition for details).
178

179 **Calculation of CFU per IJ.** The CFU per IJ assessment was adapted from (Murfin *et*
180 *al.*, 2019). IJ suspension from water-trap was added to a sterile 1.5 mL microfuge tubes
181 (Eppendorf, Germany) and centrifuged at 634 g for two minutes to concentrate the
182 nematodes. The supernatant was removed using a vacuum, and 1 mL of a 1% bleach
183 solution was added to the pellet, which was incubated for 2 min at room temperature to
184 surface sterilize IJs. IJs were washed thrice with and resuspended in 1 mL of LB
185 medium, and their concentration was assessed by viewing 2 µL spots under a
186 stereoscope. 200 IJs were then resuspended in 250 µL of LB broth. IJs were
187 homogenized for 2 minutes using a hand-held motor-driven grinder and Kontes
188 polypropylene microtube pellet pestle. Serial dilutions of the homogenate were then
189 plated on LB agar plates with 50 µg/mL kanamycin.
190
191 **Soil Challenge of IJ colonization.** IJ suspensions were transferred to sterile 15 mL
192 conical tubes and centrifuged at 3000 rpm for 2 minutes to form a pellet. IJs were then
193 resuspended in 10 mL of M9 buffer (Stiernagle, 2006) and split into two 50 mL culture
194 flasks, 5 mL each. The concentrations of IJs in each flask were assessed under a
195 stereoscope and recorded. For each plate, a 1:5 dilution of M9-soaked soil (5 g Miracle-
196 Gro Potting Mix in 45 mL of M9 incubated at room temperature overnight, approximately
197 8000 CFU/µL) was filtered through a Whatman paper and added to one of the flasks to
198 simulate microbial challenge. Weekly, the colonization frequency for each flask was
199 measured via fluorescence microscopy by counting the number of colonized and
200 uncolonized worms. 200 IJs were removed from the flask, paralyzed with a 1:100

201 dilution of a 2 mM levamisole stock, concentrated in 10 μL of sterile water, and imaged
202 on 5% agar pads.
203
204 **Microscopy and Image Acquisition.** IJ nematodes were concentrated from water-
205 traps by centrifugation at 1761 g for one minute and immobilized by addition of
206 levamisole to a final concentration of 5 mM. The nematodes were mounted onto 5%
207 agarose in water and covered with a cover glass (Cao *et al.*, 2021) . Photomicrographs
208 and videos were acquired using Zeiss Imager Z2 microscope equipped with Apotome 2
209 and Axiocam 506 mono using Zen 2 Blue software.
210
211 **Results**
212 ***E. coli* Nissle cells interact with coelomocytes of *S. hermaphroditum* IJ.**
213 Using fluorescence microscopy, we observed that mScarlet-I-expressing *E. coli* Nissle
214 cells localize to at least four 'spots' close to the midbody of *S. hermaphroditum* IJs, with
215 two spots on the posterior dorsal side and two on the anterior ventral side
216 (approximately 5-10 μm in diameter) (Fig. 2A and 2B). Z-stack imaging for these four
217 'spots' showed that each consists of a pair of large ovoid cells (Fig. 2D, Video S1).
218 Within each cell, the cytosol, containing lysates from fluorescent bacteria, surrounds a
219 dark center which features the nuclease (Fig. 2D). Based on the morphology and
220 localization of these cells, we identify them as the coelomocytes, a cell type known to
221 serve defense and immune functions in invertebrates including some nematode species
222 (Engelmann *et al.*, 2005; Tahseen, 2009; Smith *et al.*, 2010). Nematode coelomocytes
223 are known to have diverse morphologies, sizes, and numbers. The morphology of

224 coelomocytes ranges from oval-shaped to star-shaped; the sizes of these cells correlate
225 with the size of the animals (from less than 1 mm to a few meters long). They are
226 proposed to participate in the up-take and scavenging of proteins circulating in the
227 pseudocoelomic space. Whether or not the coelomocytes could engulf bacterial cells
228 depends on the species of nematode (Tahseen, 2009). For instance, *C. elegans*
229 coelomocytes were found to have endocytosed toxins, such as nematode-expressed
230 green fluorescent proteins that circulate in the body cavity (Fares and Greenwald,
231 2001). In contrast, the mammalian parasitic nematode *Ascaris suum* was observed to
232 phagocytose living bacterial cells in their coelomocytes (Tahseen, 2009). Neither the
233 morphology nor the function of *Steinernema* coelomocytes has been previously
234 documented. As expected, we observed that *S. hermaphroditum* coelomocytes are
235 oval-shaped, like other *Rhabditis* nematodes; rod-shaped bacterial cells were visible in
236 the coelomocytes (Fig. 2C, 2E, and 2F) consistent with the model that bacteria are
237 trapped and lysed in the lysosomes. These observations suggest the phagocytotic and
238 endocytic functions of *Steinernema* coelomocytes directly towards invading *E. coli*
239 Nissle which causes an active immune response in the host nematode.
240
241 ***E. coli* Nissle cells localize and proliferate in the IJ intestine**.
242 As typical of bacterivorous nematodes, the intestine of *Steinernema* serves as the
243 largest organ facilitating microbial interactions where bacteria can be engulfed,
244 digested, or colonized (McGhee, 2007) . Prior to IJ development, EcN cells are engulfed
245 and digested in the intestinal lumen of *S. hermaphroditum* juveniles (Fig. S1). When the
246 intestinal lumen collapses and closes during IJ development, we observe EcN cells

247 attaching to the posterior end of the IJ intestine within multiple small ‘pockets’. We term
248 these structures, which were not previously identified, as ‘vacuoles’ (Fig. 3A and 3B).
249 Within the same IJ, EcN cells localize and proliferate in one or more intestinal vacuoles
250 (Fig. 3B), showing their role as reservoirs for invading microbes. Individual bacterial
251 cells were also observed to ‘escape’ from the vacuoles, pass through the anus, and
252 eventually enter the space in between the internal cuticle and a layer of growing exterior
253 cuticle (Fig 3B, panel c). This process may be caused by either bacterial motility (such
254 as swimming), or by the movement of the nematode intestine during IJ development as
255 it collapses and squeezes out the bacteria accumulated inside the intestinal lumen.
256 Intestinal colonization was specific to liver-kidney agar condition lacking *X. griffiniae*
257 symbiotic bacteria (Fig. 3C), suggesting that the nutritional profile of liver-kidney agar
258 and the specific features of the *E. coli* Nissle strain are essential. The addition of the *X.*
259 *griffiniae* symbiont was also shown to inhibit intestinal colonization of EcN (Fig. 3C),
260 possibly due to its ability to antagonize *E. coli* growth by producing antimicrobial
261 molecules (Dreyer *et al.*, 2018). Overall, EcN is likely a mild and opportunistic pathogen
262 of *S. hermaphroditum,* and some EcN cells are able to gain resistance to the host
263 immune response by invading and persisting in the IJ intestine.
264
265 ***E. coli* Nissle cells aggregate and migrate in the IJ inter-cuticular space**.
266 *S. hermaphroditum* IJs can have up to two cuticle layers: an inner collagenous cuticle
267 similar to that seen in other developmental stages (Wolkow and Hall, 2011), and
268 sometimes an outer cuticle that is known to protect the animal from pathogenic
269 microbes (Timper and Kaya, 1989) . We observed aggregates of bacterial cells trapped

270 in the posterior end of the inter-cuticular space (Fig. 4A and 4B; Fig. S3). Cuticular
271 association of EcN is either exclusively localized to the posterior side or co-localized at
272 both the posterior and anterior sides (Fig. S3). No IJ was only associated at the anterior
273 cuticle without posterior colonization, confirming the directionality of colonization from
274 the posterior to the anterior; thus, this event is likely to follow intestinal colonization. Like
275 colonization of the posterior intestinal vacuoles, inter-cuticular colonization was also
276 specific to growth on liver-kidney agar without the presence of any *X. griffiniae*
277 symbionts. This is consistent with our hypothesis that these two colonization
278 phenotypes are correlated (Fig. 3C; Fig. 4C). Along this line of evidence, we also
279 observed the co-occurrence of EcN cells during intestinal and cuticular colonization
280 (Fig. S3).
281
282 **Proteins from *E. coli* cell lysates persist in the IJ inter-cuticular space.**
283 We observed live EcN cells that were temporarily maintained in the IJ cuticular space
284 for around two weeks before they were observed to lyse. Lysis is marked by the
285 presence of both individual bacterial cells and a smear of bright fluorescence from the
286 mScarlet reporter (Fig. 5A). Eventually, only mScarlet proteins contained in the bacterial
287 lysates remained in the inter-cuticular space (Fig. 5B). Surprisingly, diffused mScarlet is
288 observed in the inter-cuticular in IJs grown under all conditions (not specific to *E. coli*
289 strain, growth media, or the presence of symbiotic *X. griffiniae* bacteria) (Fig. 5C). This
290 observation suggests that in addition to living bacterial colonization as described above,
291 other mechanisms could cause bacterial proteins to be expelled and trapped in the
292 inter-cuticular space.

293

294 To test a potential environmental engineering concept, we investigated if fluorescent
295 proteins contained in the EcN lysates in the nematode cuticle can persist long-term
296 when the IJs were challenged by external soil microbes (Fig. 6; Fig. S4). Although
297 cuticle growth and colonization percentages varied among a different replicates and
298 experiments within populations of IJs, bacterial proteins in the lysates remained in the
299 cuticle over eight weeks of IJ aging (Fig. 6; Fig. S4). Overall, soil challenge did not
300 significantly affect mScarlet persistence in the cuticle. The long-term persistence of
301 bacterial proteins in soil-dwelling IJs presents a promising opportunity to utilize IJs as
302 carriers of engineered bacterial components in soil environments.

303

304 **Discussion**

305 In this research, we found EcN cells interacting with four pairs of *S. hermaphroditum*
306 coelomocytes. In model organism *C. elegans* that has the most characterized anatomy
307 and immune system among nematode species, three pairs of coelomocytes are
308 attached to the pseudocoelomic space with three layers of defense preventing bacterial
309 access: the grinding of bacteria by the pharynx, multiple layers of cuticles, and an active
310 immune system defending against the invading microbes (Altun and Hall, 2005). Here,
311 we show that *E. coli* Nissle can access *S. hermaphroditum* coelomocytes, suggesting
312 that at least one of the three barriers fails to defend against EcN. Invertebrate immune
313 cells are known to interact with both mutualistic and pathogenic symbionts. For
314 instance, in the Hawaiian bobtail squid *Euprymna scolopes,* symbiotic *Vibrio fischeri*
315 bacteria adhere to a single blood-cell type, the haemocytes, with less affinity in

316 comparison to pathogen adherence (Nyholm *et al.*, 2009). In *S. hermaphroditum*, the
317 mutualistic symbiont *X. griffiniae* has not been observed to interact with host
318 coelomocytes, suggesting that the role of these immune cells may be specific to
319 pathogens.
320
321 EcN cells were also found enclosed in the posterior intestinal pockets of IJs. These
322 pockets, which we term 'vacuoles', are shown in both conventional IJs (those caught
323 from nature and grown only through the natural insect infection process) and axenic IJs
324 (those that are gnotobiotic). This suggests that neither the presence of EcN nor the
325 absence of *Xenorhabdus* symbionts causes the formation of these structures. Based on
326 the size and morphology of the debris present in the intestinal vacuoles, these void
327 spaces are likely to have formed via lysis of the intestinal cells or organelles (Fig. 3B,
328 panel a; Fig. S1; Video S2 and S3). Our data suggest that the posterior end, similar to
329 the anterior end of the IJ intestine (Chaston *et al.*, 2013) , features compartments that
330 are specific to the colonization and proliferation of certain environmental microbes.
331 In previous studies, environmental microbes were found in *S. scapterisci* in the 'inter-
332 cuticular space', defined as the space in between the inner cuticle of J2 and J3 larvae
333 (Bonifassi *et al.*, 1999) . Those rod-shaped bacteria, reported as 'contaminants', were
334 thought to be wrapped into the J3 cuticle during nematode growth and molting (Fig. 7A).
335 Note that in this research, EcN cells are localized to the space in between the
336 collagenous inner cuticle and the outer cuticle. Based on our observations, we propose
337 that the bacteria enter the inter-cuticular space after being expelled from the intestine
338 (Fig. 4A and 4B). Within the inter-cuticular space, EcN cells were observed to migrate

339 from the posterior to the anterior side where they form aggregates, proving that these
340 bacterial cells are indeed living. What causes the lysis of EcN cells in the cuticle is
341 unknown, some possibilities include host nematode immune response (clear a
342 pathogen), or an exhaustion of nutrients in the inter-cuticular space.
343
344 **Conclusion**
345 In this work, we report previously unidentified cells and tissues within *Steinernema*
346 nematodes where *E. coli* Nissle (EcN) can localize, proliferate, and lyse. We
347 characterized sequential EcN localization within infective juveniles (IJs), including
348 immune cells (coelomocytes), posterior intestinal vacuoles, and the inter-cuticular space
349 between the interior collagenous cuticle and the exterior cuticle (Fig. 7B). Remarkably,
350 mScarlet proteins from EcN lysates persisted within the inter-cuticular space for over
351 eight weeks under non-sterile soil conditions. This observation challenges the paradigm
352 that environmental microbes are passively “wrapped” within molting nematode cuticles
353 (Fig. 7A). Instead, our findings demonstrate that EcN can actively associate with soil-
354 dwelling *Steinernema* in a tissue-specific manner in a niche that is separate from the
355 nematode’s natural symbiont. During EcN invasion, the immune response of
356 *Steinernema hermaphroditum* engages the pseudocoelom, intestinal structures, and
357 cuticle.

358 Despite the potential of binary symbiosis systems in environmental engineering, they
359 remain underexplored. Engineering vertically transmitted symbionts or endosymbionts,
360 which reside in host cell cytosol and are maternally passed through oocytes (Bright and
361 Bulgheresi, 2010) , is technically challenging. In contrast, horizontally transmitted

362 microbiomes—such as the association of *S. hermaphroditum* with *Xenorhabdus*
363 *griffiniae* and EcN—are acquired extracellularly from the environment in each
364 generation. This mode of symbiont acquisition offers key advantages for microbial
365 bioengineering: symbiotic bacteria can be cultured and genetically modified *ex vivo*,
366 then easily re-associated with the host. This enables the use of engineered microbes to
367 monitor microenvironments within host tissues or to assess external environmental
368 conditions within relevant ecosystems.

369 **Acknowledgements**

370 We thank Tara Chari for sharing the *E. coli* Nissle strain with constitutive mScarlet-I
371 reporter used in this research. We thank Heidi Goodrich-Blair, Jennifer Heppert, and
372 Omar Alani for sharing the *Xenorhabdus* bacterial strains used in this research. We
373 thank Paul Sternberg for providing space and equipment support.
374 MC, VC and JPM were supported in part by the Resnick Sustainability Institute. MC was
375 also supported by Carnegie Institution for Science. JPM and RMM were also supported
376 in part by the Institute for Collaborative Biotechnologies through contract W911NF-19-
377 D-0001 from the U.S. Army Research Office. The content of the information on this
378 page does not necessarily reflect the position or the policy of the Government, and no
379 official endorsement should be inferred.

380

381 **Authors contributions**

382 MC and JPM oversaw and conceptualized the project. JPM, VC, and MC acquired
383 preliminary data on *E. coli* colonization in *Steinernema* nematode cuticle that led to the
384 initiation of the project. VC and MC designed the and performed experiments, collected

and analyzed data with JPM's assistance. MC and VC wrote the manuscript. JPM and RMM edited the manuscript. RMM supervised the project and mentored VC, JPM, and MC.

388 **Figure 1:** *Steinernema hermaphroditum* intestine provides specific niches for host-
389 microbe interactions. (A). *S. hermaphroditum* life cycle and symbiont colonization in
390 specific tissues at the anterior intestine. (B). *S. hermaphroditum* IJ that has the potential
391 to interact with both mutualistic and pathogenic microbes. (C). Biphasic lifestyle of
392 *E. coli* that oscillates between associating with mammalian gut and persisting in the soil,
393 which provides an opportunity to interact with soil-dwelling *Steinernema* nematodes. Bb:
394 basal bulb; AIC: anterior intestinal caecum; PIV: pharyngeal intestinal valve.
395

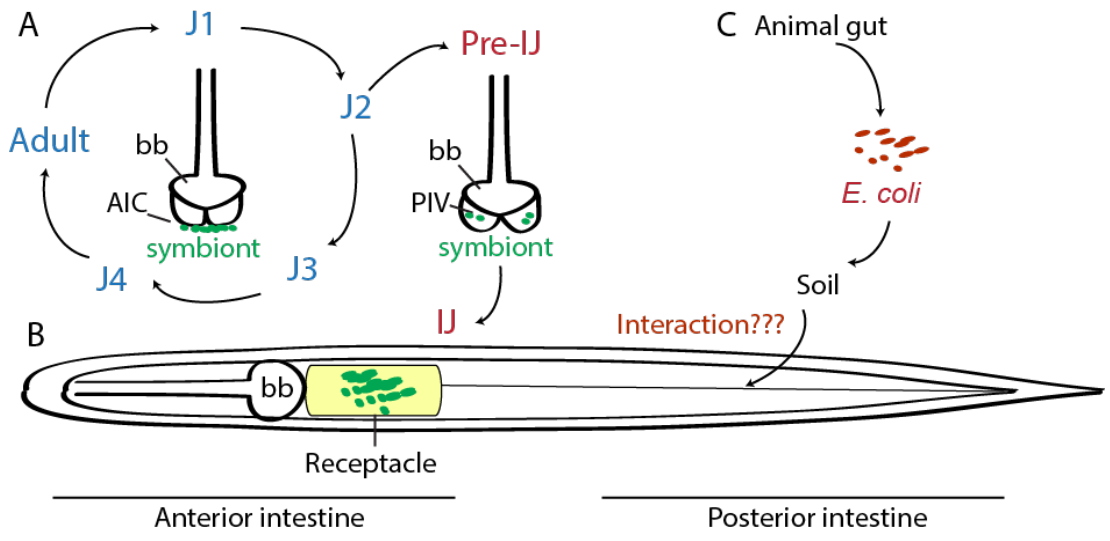

396

Figure 2: *E. coli* Nissle localizes in the *Steinernema hermaphroditum* IJ coelomocytes. (A). A schematic diagram showing *S. hermaphroditum* IJs has at least four pairs of coelomocytes. (B) and (C). A representative IJ showing *E. coli* Nissle localized and lysed within coelomocytes. (D). Each ovoid coelomocyte structure contains two cells. (E) and (F). Rod-shaped bacterial cells are observed inside of the coelomocyte cytosol. Scale bars in panel D, E, and F equals to 20 µm. (Also see Video S1).

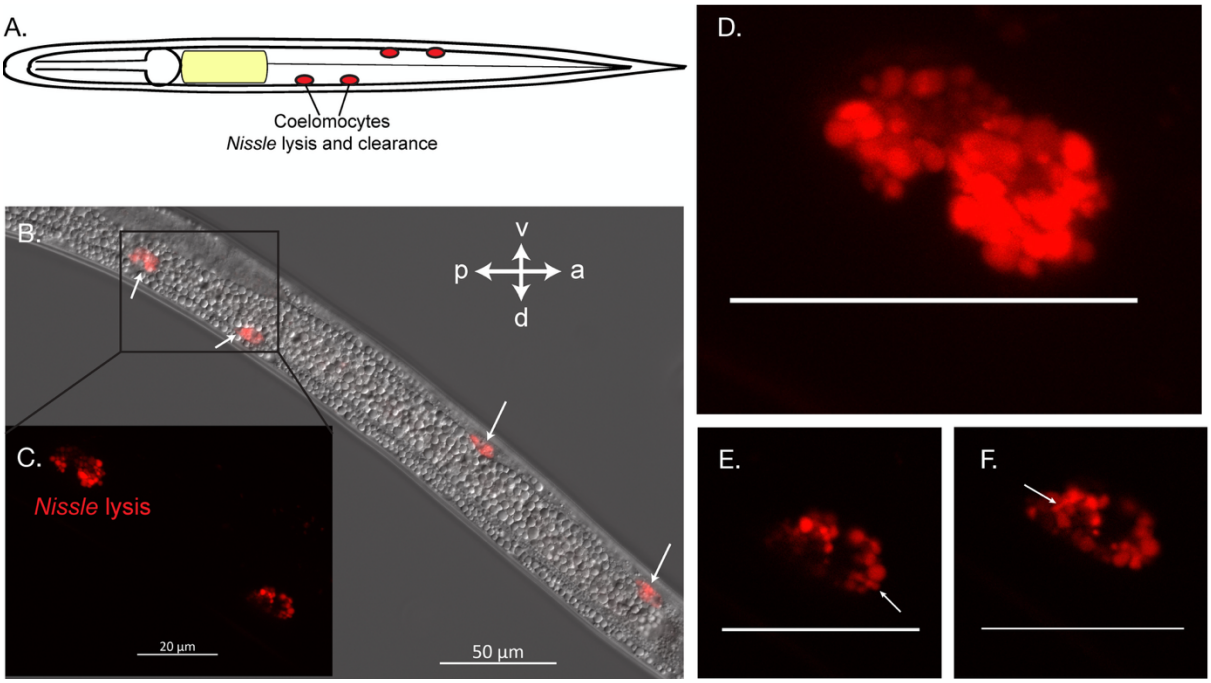

405 **Figure 3**: *E. coli* Nissle localizes in the *S. hermaphroditum* intestinal lumen and
406 vacuoles. (A). A schematic diagram showing *E. coli* Nissle invading nematode intestine
407 and proliferating in the intestinal vacuoles. (B). A representative IJ showing intestinal
408 colonization of bacteria: an empty intestinal vacuole containing cell or organelle debris-
409 looking substance (a); bacterial colonization in the IJ intestinal vacuoles (b); bacterial
410 cells escape from the posterior intestinal opening (c). (C). Quantification of intestinal
411 colonization frequency of *E. coli* strains: Nissle (Nis), *E. coli* CSH50 (CSH), BW25113
412 (BW) under nutritional conditions of either liver-kidney (LK) or lipid agar (LA).
413 Treatments were either with (+) or without (-) symbiont *X. griffiniae.* Numbers in the
414 parenthesis indicate the number of animals screened in each treatment.

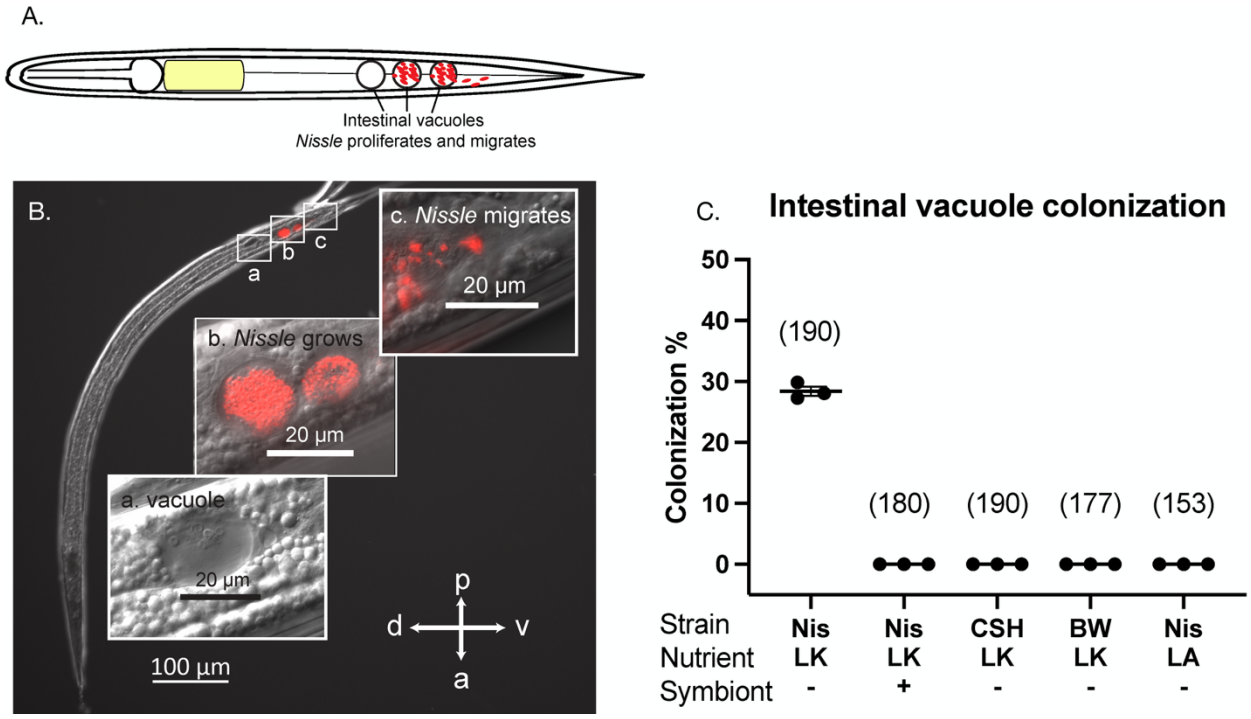

415

416

Figure 4: Intercuticular colonization of *E. coli* Nissle. (A). A schematic diagram showing *E. coli* Nissle colonizes in the intercuticular space in the IJs. (B). A representative IJ showing intercuticular proliferation of bacteria: the head region (a) and the tail region (b). Arrow indicates the intestinal vacuole colonization observed in the same IJ with cuticular colonization. (C). Quantification of cuticular proliferation frequency of *E. coli* strains: Nissle (Nis), *E. coli* CSH50 (CSH), BW25113 (BW) under nutritional conditions of either liver-kidney (LK) or lipid agar (LA). Treatments were either with (+) or without (-) symbiont *X. griffiniae.* Numbers in the parenthesis indicates the number of animals screened in each treatment.

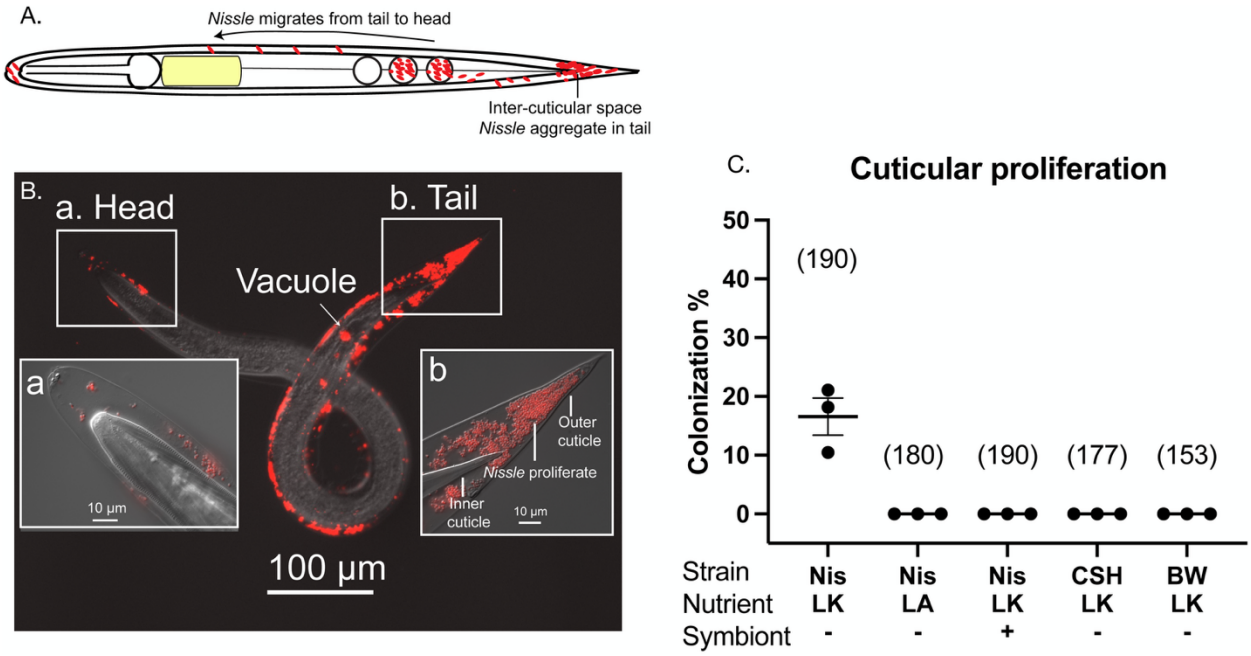

429 **Figure 5:** *E. coli* Nissle cells lyse in the IJ inter-cuticular space. (A). A representative IJ
430 (2 weeks post trapping) showing transitional stage in which bacterial cells and mScarlet
431 contained in cell lysate co-localize in the inter-cuticular space. (B). Diffused
432 fluorescence from mScarlet expressing *E. coli* cells is found in symbiont-colonized IJs.
433 (C). Quantification of cuticular diffusion of mScarlet expressing *E. coli* strains: Nissle
434 (Nis), *E. coli* CSH50 (CSH), BW25113 (BW) under nutritional conditions of either liver-
435 kidney (LK) or lipid agar (LA). Treatments were either with (+) or without (-) symbiont *X.*
436 *griffiniae.* Numbers in the parenthesis indicates the number of animals screened in each
437 treatment.

438 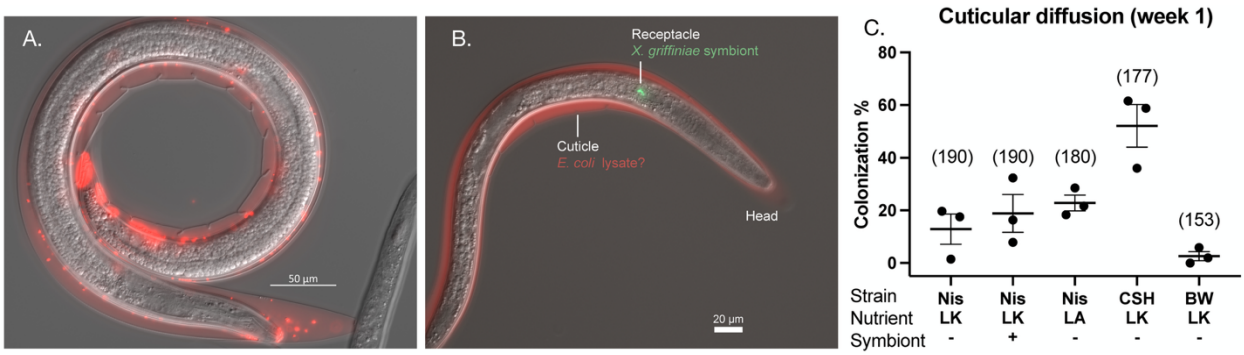

439

440

441

442 **Figure 6:** Proportion of developed outer cuticles and cuticularly colonized IJs as a
443 fraction of total IJs with and without soil challenge. Developed cuticles (noted as
444 'developed') include those with fully developed, less developed, or broken outer
445 cuticles. The presence of *E. coli* Nissle produced mScarlet proteins in IJ cuticles (noted
446 as 'colonized') was assessed by fluorescence microscopy. (A). IJ cuticle development
447 and colonization of mScarlet protein in the inter-cuticular space over three weeks. (I),
448 (II), and (III) represents three biological replicates. (B). Cuticle development and
449 cuticular mScarlet colonization frequency over ten weeks. (IV), (V), and (VI) represent
450 three biological replicates. (C). A comparison of IJ cuticle development and cuticular
451 colonization by mScarlet in week 8 and week 9 with and without challenge by non-
452 sterile soil.

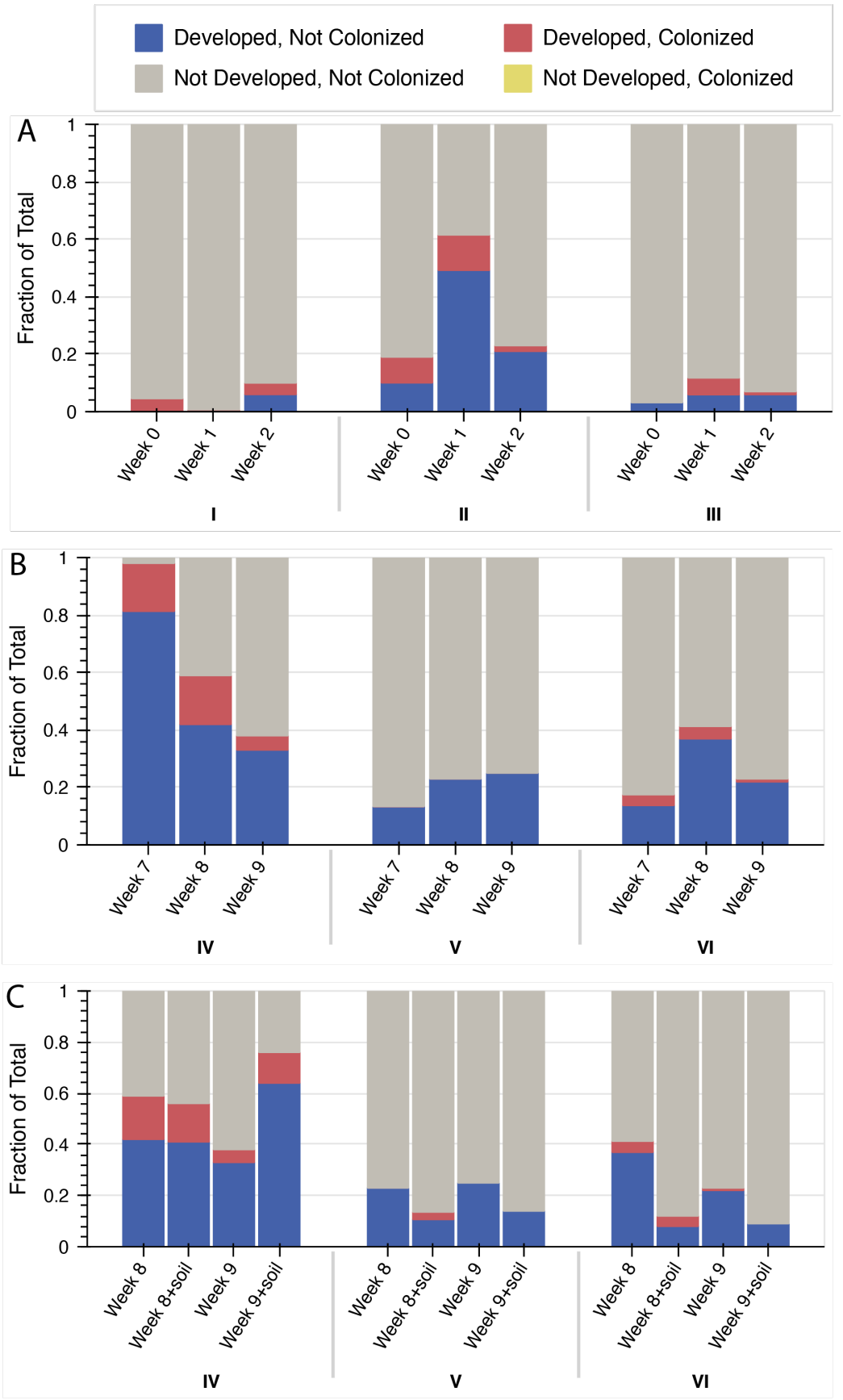
Developed, Not Colonized
Developed, Colonized
Not Developed, Not Colonized
Not Developed, Colonized
A
Fraction of Total
1
0.8
0.6
0.4
0.2
0
Week 0
Week 1
Week 2
I
II
III
B
Week 7
Week 8
Week 9
IV
V
VI
C
Week 8
Week 8+soil
Week 9
Week 9+soil

453

454 **Figure 7:** Hypothetical models of *E. coli* Nissle interaction in *S. hermaphroditum*. (A). A
455 hypothetical model based on a previous publication of *S. scapterisci* cuticular microbes
456 (Bonifassi *et al.*, 1999) : environmental microbes attaching to the inner cuticle during IJ
457 formation. (B). Current hypothetical model based on data from this research: *E. coli*
458 Nissle possibly causes mild infection in *S. hermaphroditum*.

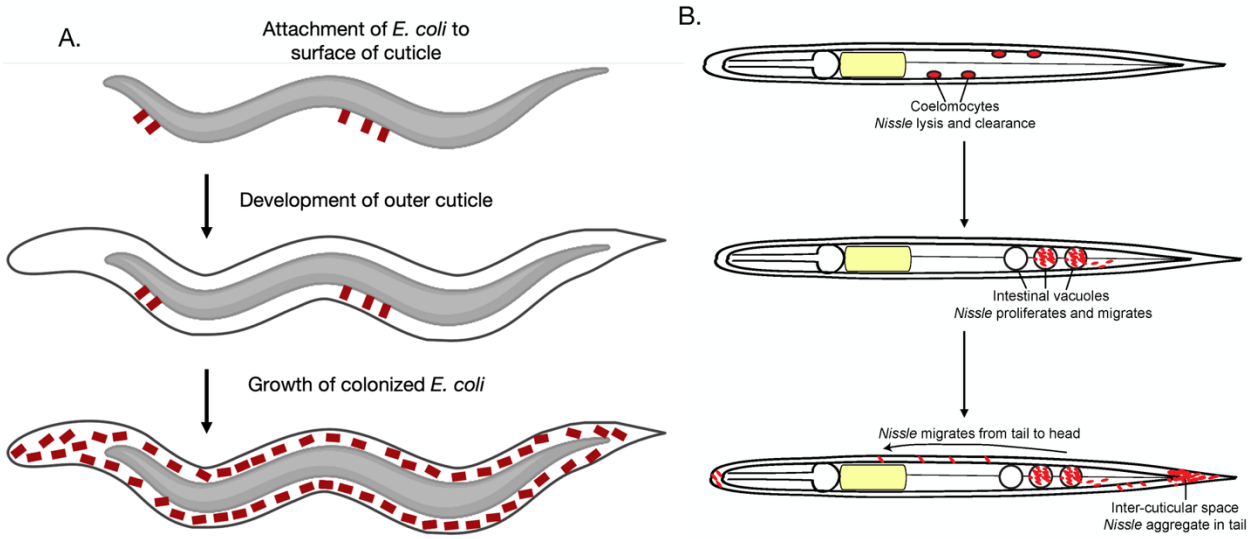

459
460
461

462 **References**

463

464 Altun, Z.F. and Hall, D.H. (2005) WormAtlas Hermaphrodite Handbook - Coelomocyte
465 System. *WormAtlas*.

466 Baquero, F., Coque, T.M., Galán, J.C., and Martinez, J.L. (2021) The Origin of Niches
467 and Species in the Bacterial World. *Front Microbiol* **12**: 657986.

468 Bonifassi, E., Saux, M.F.-L., Boemare, N., Lanois, A., Laumond, C., and Smart, G.
469 (1999) Gnotobiological Study of Infective Juveniles and Symbionts of *Steinernema*
470 scapterisci: A Model to Clarify the Concept of the Natural Occurrence of Monoxenic
471 Associations in Entomopathogenic Nematodes. *J Invertebr Pathol* **74**: 164–172.

472 Bracho, O.R., Manchery, C., Haskell, E.C., Blanar, C.A., and Smith, R.P. (2016)
473 Circumvention of Learning Increases Intoxication Efficacy of Nematicidal Engineered
474 Bacteria. *Acs Synth Biol* **5**: 241–249.

475 Bright, M. and Bulgheresi, S. (2010) A complex journey: transmission of microbial
476 symbionts. *Nat Rev Microbiol* **8**: 218–230.

477 Cao, M., Schwartz, H.T., Tan, C.-H., and Sternberg, P.W. (2021) The
478 entomopathogenic nematode *Steinernema hermaphroditum* is a self-fertilizing
479 hermaphrodite and a genetically tractable system for the study of parasitic and
480 mutualistic symbiosis. *Genetics* **220**:.

481 Chaston, J.M., Murfin, K.E., Heath-Heckman, E.A., and Goodrich-Blair, H. (2013)
482 Previously unrecognized stages of species-specific colonization in the mutualism
483 between *Xenorhabdus* bacteria and *Steinernema* nematodes: Species-specific host
484 colonization by Xenorhabdus. *Cell Microbiol* **15**: 1545–1559.

485 Dale, C. and Moran, N.A. (2006) Molecular Interactions between Bacterial Symbionts
486 and Their Hosts. *Cell* **126**: 453–465.

487 Dreyer, J., Malan, A.P., and Dicks, L.M.T. (2018) Bacteria of the Genus *Xenorhabdus*, a
488 Novel Source of Bioactive Compounds. *Front Microbiol* **9**: 3177.

489 Elsas, J.D. van, Semenov, A.V., Costa, R., and Trevors, J.T. (2010) Survival of
490 *Escherichia coli* in the environment: fundamental and public health aspects. *ISME J*
491 **5**: 173–183.

492 Engelmann, P., Cooper, E.L., and Németh, P. (2005) Anticipating innate immunity
493 without a Toll. *Mol Immunol* **42**: 931–942.

494 Fares, H. and Greenwald, I. (2001) Genetic Analysis of Endocytosis in Caenorhabditis
495 elegans: Coelomocyte Uptake Defective Mutants. *Genetics* **159**: 133–145.

496 Flores-Lara, Y., Renneckar, D., Forst, S., Goodrich-Blair, H., and Stock, P. (2007)
497 Influence of nematode age and culture conditions on morphological and physiological
498 parameters in the bacterial vesicle of *Steinernema carpocapsae* (Nematoda:
499 Steinernematidae). *J Invertebr Pathol* **95**: 110–118.

500 Halleran, A.D., Swaminathan, A., and Murray, R.M. (2018) Single Day Construction of
501 Multigene Circuits with 3G Assembly. *Acs Synth Biol* **7**: 1477–1480.

502 Hwang, I.Y., Koh, E., Wong, A., March, J.C., Bentley, W.E., Lee, Y.S., and Chang, M.W.
503 (2017) Engineered probiotic *Escherichia coli* can eliminate and prevent
504 *Pseudomonas aeruginosa* gut infection in animal models. *Nat Commun* **8**: 15028.

505 Iverson, S.V., Haddock, T.L., Beal, J., and Densmore, D.M. (2016) CIDAR MoClo:
506 Improved MoClo Assembly Standard and New *E. coli* Part Library Enable Rapid
507 Combinatorial Design for Synthetic and Traditional Biology. *ACS Synth Biol* **5**: 99–
508 103.

509 Maire, J., Parisot, N., Ferrarini, M.G., Vallier, A., Gillet, B., Hughes, S., et al. (2020)
510 Spatial and morphological reorganization of endosymbiosis during metamorphosis
511 accommodates adult metabolic requirements in a weevil. *Proc Natl Acad Sci* **117**:
512 19347–19358.

513 McGhee, J. (2007) The C. elegans intestine. *WormBook* 1–36.

514 Murfin, K.E., Chaston, J., and Goodrich-Blair, H. (2012) Visualizing bacteria in
515 nematodes using fluorescent microscopy. *J Vis Exp Jove*.

516 Murfin, K.E., Ginete, D.R., Bashey, F., and Goodrich-Blair, H. (2019) Symbiont-
517 mediated competition: *Xenorhabdus bovienii* confer an advantage to their nematode
518 host Steinernema affine by killing competitor Steinernema feltiae. *Environ Microbiol*
519 **21**: 3229–3243.

520 Nyholm, S.V. and McFall-Ngai, M.J. (2021) A lasting symbiosis: how the Hawaiian
521 bobtail squid finds and keeps its bioluminescent bacterial partner. *Nat Rev Microbiol*
522 **19**: 666–679.

523 Nyholm, S.V. and McFall-Ngai, M.J. (1998) Sampling the light-organ microenvironment
524 of *Euprymna scolopes*: description of a population of host cells in association with the
525 bacterial symbiont *Vibrio fischeri*. *Biological Bulletin* **195**: 89–97.

526 Nyholm, S.V., Stewart, J.J., Ruby, E.G., and McFall-Ngai, M.J. (2009) Recognition
527 between symbiotic *Vibrio fischeri* and the haemocytes of Euprymna scolopes.
528 *Environ Microbiol* **11**: 483–493.

529 Ogier, J.-C., Pagès, S., Frayssinet, M., and Gaudriault, S. (2020) Entomopathogenic
530 nematode-associated microbiota: from monoxenic paradigm to pathobiome.
531 *Microbiome* **8**: 25.

532 Rutter, J.W., Ozdemir, T., Quintaneiro, L.M., Thomas, G., Cabreiro, F., and Barnes,
533 C.P. (2019) Detecting changes in the *Caenorhabditis elegans* intestinal environment
534 using an engineered bacterial biosensor. *Biorxiv* 717215.

535 Smith, L.C., Ghosh, J., Buckley, K.M., Clow, L.A., Dheilly, N.M., Haug, T., et al. (2010)
536 Echinoderm immunity. *Adv Exp Med Biol* **708**: 260–301.

537 Sonnenborn, U. (2016) *Escherichia coli* strain Nissle 1917—from bench to bedside and
538 back: history of a special *Escherichia coli* strain with probiotic properties. *FEMS*
539 *Microbiol Lett* **363**: fnw212.

540 Stiernagle, T. (2006) Maintenance of *C. elegans*. *Wormbook* 1–11.

541 Stilwell, M.D., Cao, M., Goodrich-Blair, H., and Weibel, D.B. (2018) Studying the
542 Symbiotic Bacterium *Xenorhabdus nematophila* in Individual, Living Steinernema
543 carpocapsae Nematodes Using Microfluidic Systems. *Msphere* **3**: e00530-17.

544 St-Pierre, F., Cui, L., Priest, D.G., Endy, D., Dodd, I.B., and Shearwin, K.E. (2013) One-
545 Step Cloning and Chromosomal Integration of DNA. *Acs Synth Biol* **2**: 537–541.

546 Tahseen, Q. (2009) Coelomocytes: Biology and Possible Immune Functions in
547 Invertebrates with Special Remarks on Nematodes. *Int J Zoology* **2009**: 1–13.

548 Thomas, N.M.St., Myers, T.G., Alani, O.S., Goodrich-Blair, H., and Heppert, J.K. (2024)
549 Green and red fluorescent strains of *Xenorhabdus griffiniae* HGB2511, the bacterial
550 symbiont of the nematode Steinernema hermaphroditum (India). *microPublication*
551 *Biol* **2024**: 10.17912/micropub.biology.001064.

552 Timper, P. and Kaya, H.K. (1989) Role of the second-stage cuticle of entomogenous
553 nematodes in preventing infection by nematophagous fungi. *J Invertebr Pathol* **54**:
554 314–321.

555 Tivey, T.R., Coleman, T.J., and Weis, V.M. (2022) Spatial and Temporal Patterns of
556 Symbiont Colonization and Loss During Bleaching in the Model Sea Anemone
557 Aiptasia. *Front Mar Sci* **9**: 808696.

558 Valle, I.D., Fulk, E.M., Kalvapalle, P., Silberg, J.J., Masiello, C.A., and Stadler, L.B.
559 (2021) Translating New Synthetic Biology Advances for Biosensing Into the Earth
560 and Environmental Sciences. *Front Microbiol* **11**: 618373.

561 Vivas, E.I. and Goodrich-Blair, H. (2001) *Xenorhabdus nematophilus* as a model for
562 host-bacterium interactions: rpoS is necessary for mutualism with nematodes. *J*
563 *Bacteriol* **183**: 4687–4693.

564 Wolkow, C. and Hall, D.H. (2011) WormAtlas Dauer Handbook - The Dauer Cuticle.
565 *WormAtlas*.

566

567

568

569 Supplemental Materials:

570 **Figure S1**: cell or organelle debris in the posterior intestinal vacuoles in a

571 representative infective juvenile. Black arrows: gut granules; white arrows: cell or

572 organelle debris in the intestinal vacuoles. Scale bar = 20 µm.

573

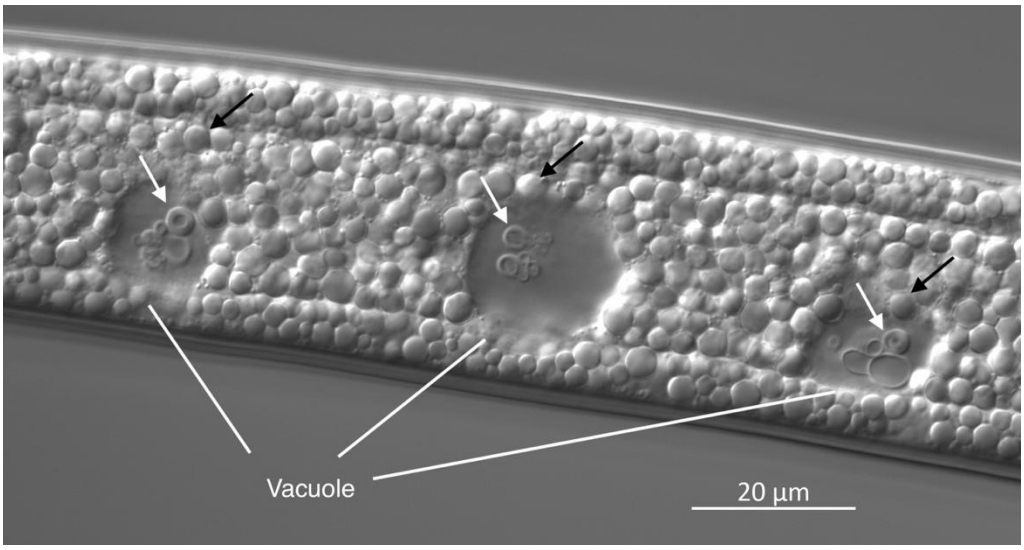

574

575
576

Figure S2: A representative *S. hermaphroditum* juvenile fed on *E. coli* Nissle. mScarlet expressing EcN cells are engulfed and digested in the intestinal lumen of J2 stage of *S. hermaphroditum.* 'P' denotes posterior end of the nematode; 'int. lumen' denotes 'intestinal lumen'; 'b.b' denotes 'basal bulb'; 'AIC' denotes 'anterior intestinal caecum'; 'PIV' denotes 'pharyngeal intestinal valve'.

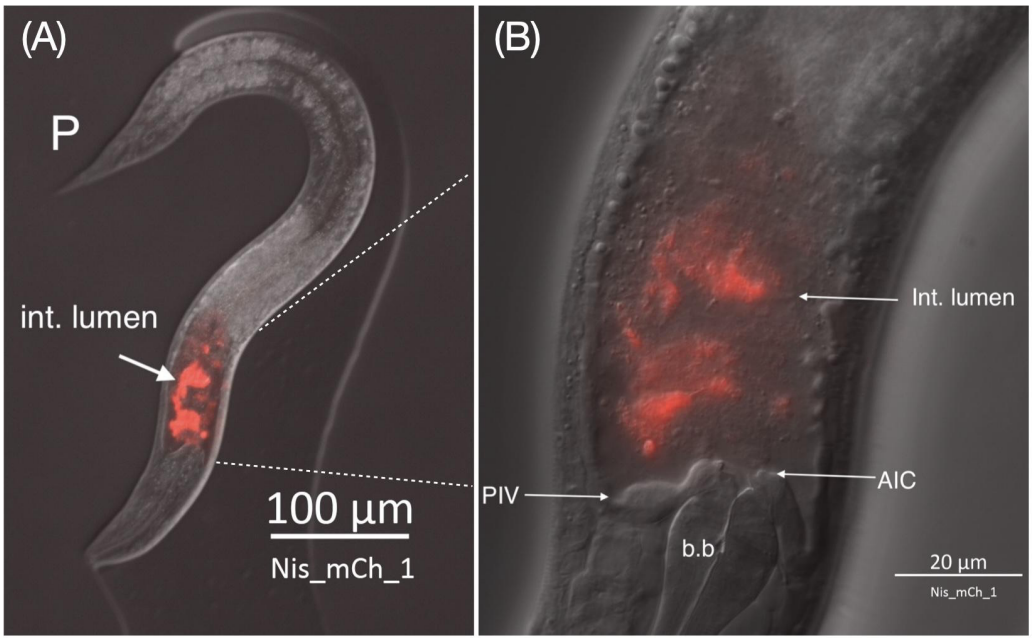

Figure S3: A profile of twenty-nine IJs with EcN colonization in the intestinal vacuoles and the inter-cuticualr space. ‘P’ denotes the posterior side of the IJ.

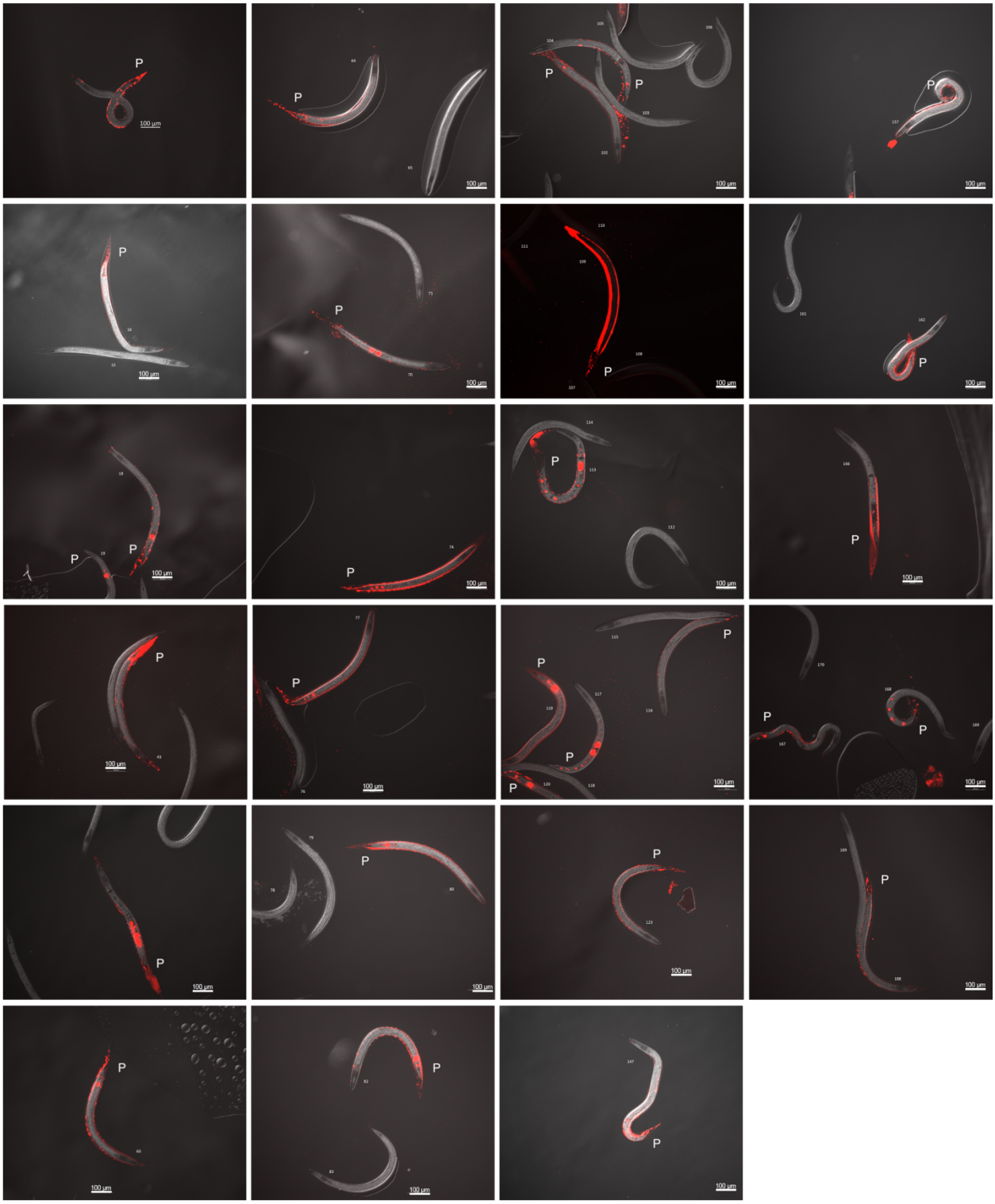

Figure S4: outer cuticle growth and bacterial protein (mScarlet) colonization in *Steinernema hermaphroditum* IJs. (A): Fractions of IJs with developed outer cuticle over 9 week's time course of experiment. (B): Fraction of developed IJs with outer cuticle that has cuticular colonization of mScarlet from EcN lysate over the 9 weeks time course of experiment.

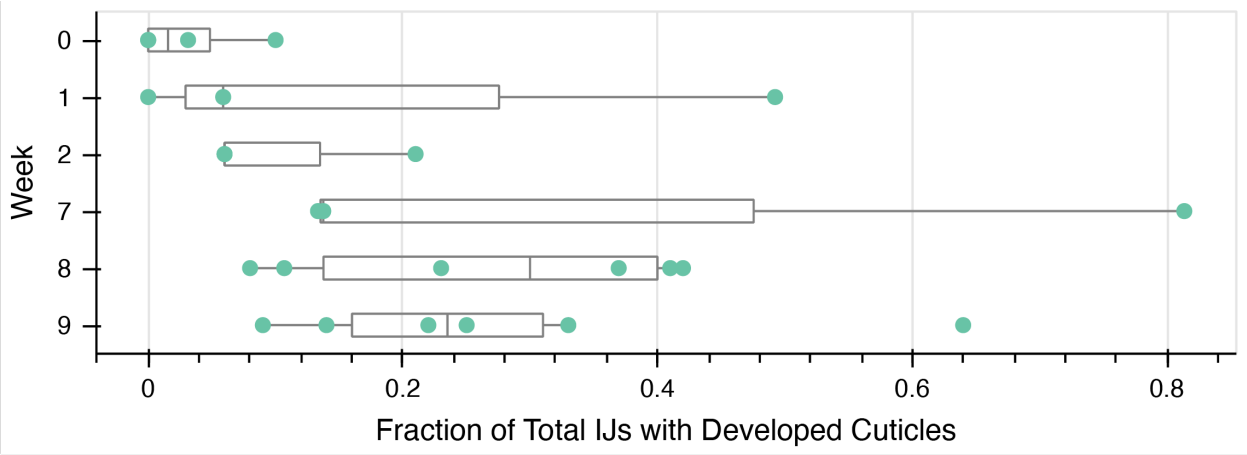

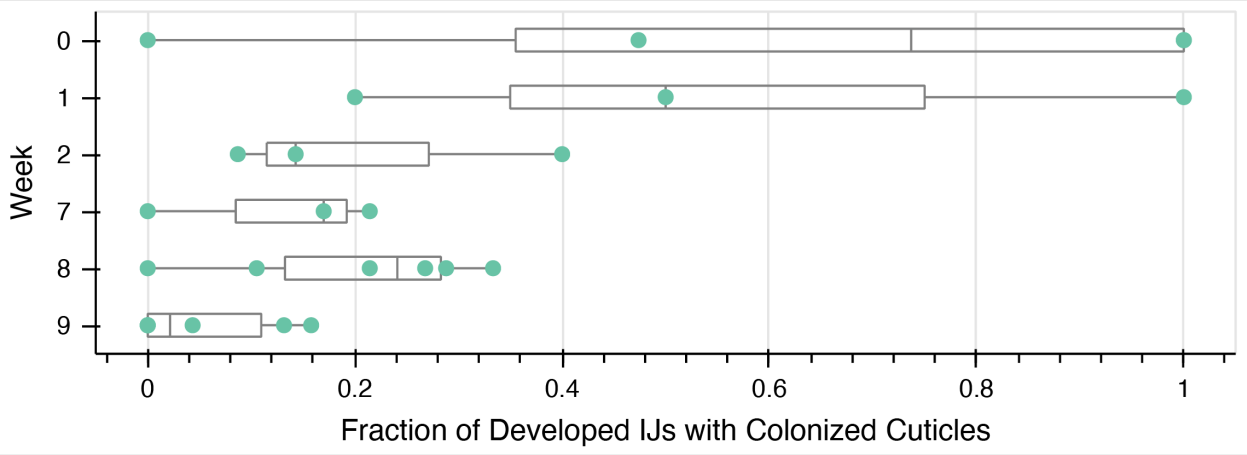

593
594 **Video S1**: bacterial lysis within the *S. hermaphroditum* coelomocytes. *E. coli* Nissle
595 expressing mScarlet is localized in the coelomocytes.
596
597 **Video S2**: intestinal cell or organelle debris in a representative intestinal vacuole.
598
599 **Video S3**: a representative IJ with two empty intestinal vacuoles housing nematode
600 organelle debris, and two vacuoles housing EcN cells expressing mScarlet.